Neuro-Oncology Advances

4(1), 1–14, 2022 | https://doi.org/10.1093/noajnl/vdab194 | Advance Access date 31 December 2021

Immune deconvolution and temporal mapping identifies stromal targets and developmental intervals for abrogating murine low-grade optic glioma formation

Amanda de Andrade Costa[†], Jit Chatterjee[†], Olivia Cobb[1], Elizabeth Cordell[1], Astoria Chao[1], Suzanne Schaeffer[1], Andrea Goldstein[1], Sonika Dahiya[2], David H. Gutmann[1]

[1]Department of Neurology, Washington University School of Medicine, St. Louis, Missouri, USA (A.A.C., J.C., O.C., E.C., A.C., S.S., A.G., D.H.G.); [2]Department of Pathology, Washington University School of Medicine, St. Louis, Missouri, USA (S.D.)

Corresponding Author: David H. Gutmann, MD, PhD, Department of Neurology, Washington University School of Medicine, Box 8111, 660 South Euclid Avenue, St. Louis MO 63110, USA (gutmannd@wustl.edu).

[†]These authors contributed equally to this work.

Abstract

Background. Brain tumor formation and progression are dictated by cooperative interactions between neoplastic and non-neoplastic cells. This stromal dependence is nicely illustrated by tumors arising in the Neurofibromatosis type 1 (NF1) cancer predisposition syndrome, where children develop low-grade optic pathway gliomas (OPGs). Using several authenticated *Nf1*-OPG murine models, we previously demonstrated that murine *Nf1*-OPG growth is regulated by T cell function and microglia Ccl5 production, such that their inhibition reduces tumor proliferation *in vivo*. While these interactions are critical for established *Nf1*-OPG tumor growth, their importance in tumor formation has not been explored.

Methods. A combination of bulk and single-cell RNA mouse optic nerve sequencing, immunohistochemistry, T cell assays, and pharmacologic and antibody-mediated inhibition methods were used in these experiments.

Results. We show that T cells and microglia are the main non-neoplastic immune cell populations in both murine and human LGGs. Moreover, we demonstrate that $CD8^+$ T cells, the predominant LGG-infiltrating lymphocyte population, are selectively recruited through increased Ccl2 receptor (*Ccr4*) expression in $CD8^+$, but not $CD4^+$, T cells, in a NF1/RAS-dependent manner. Finally, we identify the times during gliomagenesis when microglia Ccl5 production (3–6 weeks of age) and Ccl2-mediated T cell infiltration (7-10 weeks of age) occur, such that temporally-restricted Ccl2 or Ccl5 inhibition abrogates tumor formation >3.5 months following the cessation of treatment.

Conclusions. Collectively, these findings provide proof-of-concept demonstrations that targeting stromal support during early gliomagenesis durably blocks murine LGG formation.

Key points

- Selective intratumoral $CD8^+$ T cell infiltration reflects increased Ccr4 expression
- Optic glioma microglia Ccl5 production precedes Ccl2-mediated T cell infiltration
- Temporally-restricted Ccl2 or Ccl5 inhibition durably abrogates gliomagenesis

Graphical Abstract

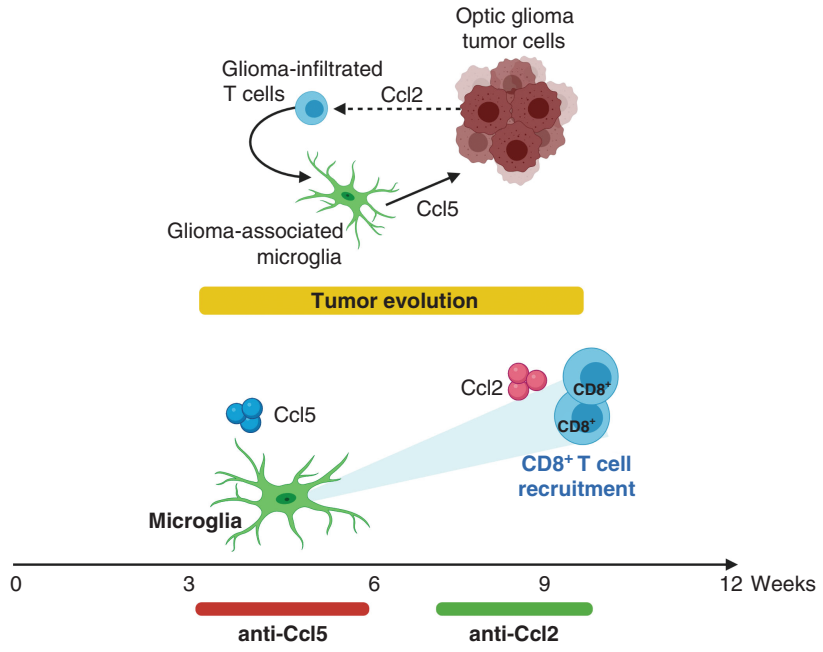

Importance of the Study

While prior studies have characterized the tumor microenvironment in pediatric low-grade brain tumors, we leveraged authenticated murine models of neurofibromatosis type 1 (*Nf1*) low-grade optic glioma to identify tumor-specific stromal cells, as well as the temporal course of microglia expansion, T cell infiltration, and paracrine factor expression during tumorigenesis. By targeting the immune axis during defined periods of tumor development, we blocked *Nf1* optic glioma formation. These findings represent a first proof-of-principle demonstration that disrupting paracrine factor circuitry during gliomagenesis is sufficient to abrogate tumor formation, suggesting future more refined chemoprevention strategies for at-risk patient groups.

Low-grade gliomas (LGGs), including pilocytic astrocytomas (PAs), are the most common pediatric brain tumors, and while associated with good overall survival, frequently cause life-long co-morbidities[1]. In contrast to other LGGs, PAs typically have low proliferative indices, lack mitotic figures, and do not progress to malignant glioma. PAs are caused by mutations that increase MAPK/ERK signaling, either from *BRAF* gene rearrangement (*KIAA1549:BRAF* fusion) or biallelic inactivation of the Neurofibromatosis type 1 (*NF1*) tumor suppressor gene[2]. This latter group of PAs typically arises within the optic pathway (optic pathway gliomas; OPGs) of children with NF1, often resulting in vision loss[3].

While both sporadic and NF1-PAs exhibit increased ERK signaling, this is usually amplified in the setting of mitogens supplied by non-neoplastic cells in the tumor microenvironment. As such, human PA cell lines are difficult to grow *in vitro* in the absence of growth factors[4] and frequently undergo oncogene-induced senescence[5–7], suggesting that the LGG cells are highly dependent upon growth/survival factors elaborated by non-neoplastic stromal cells. In this regard, as 50% of the cells in PAs are monocytes (yolk sac-derived resident brain microglia and bone marrow-derived macrophages) and, to a lesser extent, T cells[2,8]. Importantly, using authenticated murine models of *Nf1* optic glioma[9–11], we have previously shown that T cells and microglia contribute to established tumor growth[12,13], culminating in microglial elaboration of Ccl5, a paracrine factor critical for glioma cell expansion[12-14].

To define the role of non-neoplastic cells during tumor development, we took advantage of a murine *Nf1*-OPG

model with high tumor penetrance (>95%)[10] and a well-characterized time course of tumor evolution[15]. In this report, we leveraged bulk RNA sequence deconvolution, single-cell RNA sequencing (scRNAseq), and immunohistochemical analyses to define the non-neoplastic (stromal) cellular composition and its temporal development, which were then used to identify targetable paracrine factors and time windows for tumor prevention. Employing this strategy, we show that inhibition of T cell infiltration and microglial function abrogates *Nf1*-OPG formation.

Materials and Methods

Mice

Wild type (WT), *Nf1*$^{flox/flox}$ (equivalent to WT)[9], *Nf1*+/–[16], *Nf1*$^{+/R681X}$ (R681X[17]), *Nf1*$^{+/R1278P}$ (R1278P[11]), *Nf1*-OPG (*Nf1*+/– mice with somatic *Nf1* gene inactivation in neuroglial progenitors at E15.5), and *Nf1*$^{flox/R681X}$; GFAP-Cre (*Nf1*-R681X-OPG;[17]) mice were housed in a pathogen-free barrier facility with controlled light-dark cycles (12:12 h) and *ad libitum* access to food and water, and used in accordance with an approved Animal Studies protocol. *Nf1*$^{flox/flox}$ and WT mice were used interchangeably, as they are identical with respect to all parameters measured.

In vivo Mouse Treatments

Two hundred and fifty micrograms of anti-Ccl5 (R&D Systems MAB478) or anti-IgG2a control antibodies (R&D Systems) were intraperitoneally injected into *Nf1*-OPG mice daily from three to six weeks of age (WOA). In addition, seven-week-old *Nf1*-OPG mice were injected intraperitoneally five days per week for three consecutive weeks with either 2 mg/kg anti-Ccl2 or control IgG antibodies (BioXCell, BE0185, and BE0091, respectively). Mice were analyzed at 12 and 24 WOA. PLX33397 (PLX) treatments of *Nf1*-OPG mice involved replacing normal chow (AIN-76A rodent diet; Research Diet Inc.) with 275 mg/kg PLX3397-containing chow (Free Base) from four to seven WOA. PLX-treated (n = 7) or control chow (n = 8) mouse optic nerves were collected and analyzed at 24 WOA.

RNA Bulk Sequencing, Analysis, and Compilation of CNSortR

Analyses was performed using Partek Flow software, version 9.0[18]. Bulk RNA-seq reads from FAC-sorted CNS cell types[19] were aligned to the Ensembl release 95 v2 top-level assembly with STAR version 2.7.3a[20]. Sequencing performance was assessed for the total number of aligned reads, total number of uniquely aligned reads, and features detected. Gene counts and isoform expression were normalized by quantile normalization to be consistent with the previously-compiled ImmuCC reference file containing gene counts for various immune cell types[21]. Gene-specific analysis was performed using the lognormal with limma-trend shrinkage model[22], where the results were filtered by *P*-values and fold-changes, to identify the top 20 most significant marker genes for each population. Filtered gene counts were amended to the existing ImmuCC reference file and uploaded into CIBERSORTx[23]. Bulk RNA-seq data from two distinct models of murine *Nf1*-OPG (GSE102345) were analyzed and deconvoluted using CNSortR in CIBERSORTx (Supplementary Figure S1A). *Nf1*-OPG, as well as human NF1-PAs (GSE163071), were analyzed using TIMER2.0[24], which includes CIBERSORTx. *CCL2* and *CCL5* expression in human PA was determined from GSE163071 and GSE44971.

Single Cell RNA Sequencing (scRNAseq)

Nf1-OPG optic nerves were collected from eight 12-week-old mice and pooled. Mice were perfused using D-PBS with calcium, magnesium, glucose, pyruvate (ThermoFisher), and the adult brain dissociation kit (Miltenyi Biotec 130-107-677) was used to prepare single-cell suspensions. Single-cell barcoding, cDNA amplification and Gene Expression Library Construction were then performed using Chromium Single-Cell 3′ Reagent Kits v3, and10x Genomics® was used for sequencing. *Nf1*-OPG single-cell RNA sequencing data were analyzed in Partek Flow. Sequencing reads were aligned using STAR to the Ensembl annotation model. Cell quality was assessed by total reads, expressed gene count, and mitochondrial read percent. CPM normalization and PCA analysis was conducted followed by graph-based clustering using 20 principal components and the Louvain clustering algorithm. Clustering yielded 12 clusters with differentially expressed genes which were further visualized by UMAP plots generated using Euclidian distance.

Human PA Samples

De-identified human NF1-associated and sporadic PA specimens (tissue microarray) were obtained from Dr. Sonika Dahiya under an approved human studies protocol. Immunohistochemistry was performed on adjacent paraffin sections using antibodies listed in Supplementary Table S1, and detected using the Vectastain ABC kit (Vector Laboratories, Burlingame).

Immunohistochemistry

WT spleens were fixed in 4% paraformaldehyde (PFA) in 0.1M sodium phosphate buffer (pH 7.4) overnight. Following transcardial perfusion with 4% PFA, optic nerves/chiasms were dissected and post-fixed in 4% PFA. Slides were deparaffinized in xylene, subjected to antigen retrieval, and incubated overnight with the appropriate antibodies (Supplementary Table S1), followed by incubation with biotinylated secondary antibodies (1:200; Vector Laboratories, Burlingame, CA). Signals were amplified with the Vectastain ABC kit (PK4000, Vector Laboratories), developed using the Vectastain DAB kit (SK4100, Vector laboratories), and counterstained with hematoxylin. Specimens were scanned using a NanoZoomer 2.0-HT slide scanner (Hamamatsu Photonics K.K., Japan) with a 20x objective, and the percentage of immunopositive

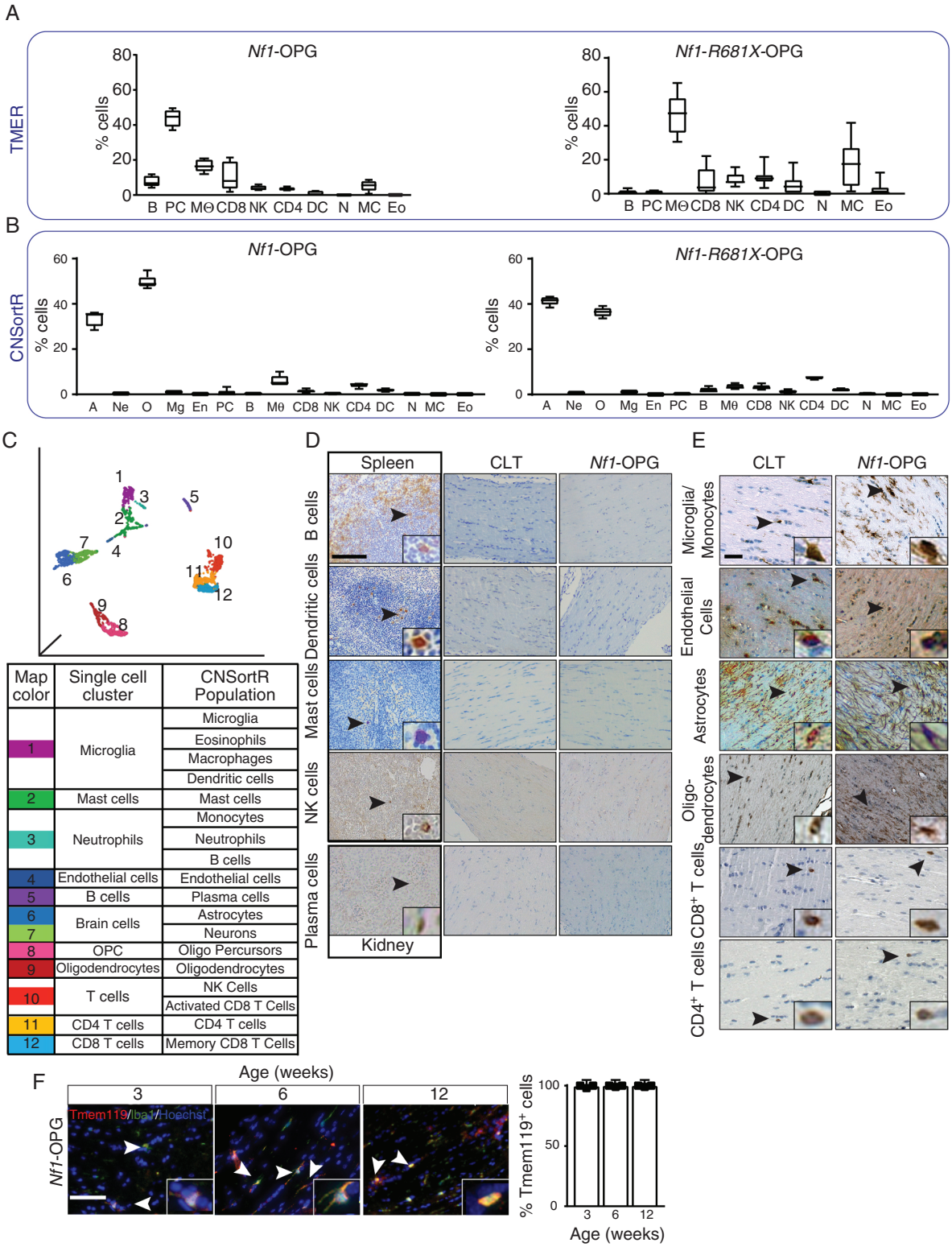

Figure 1. The *Nf1*-OPG microenvironment contains largely T cells and microglia. A, Using TIMER 2.0, *Nf1*-OPGs and *Nf1*-R618X-OPGs contain B cells (B), macrophages and monocytes (Mɵ), $CD8^+$ T cells (CD8), natural killer cells (NK), $CD4^+$ T cells (CD4), dendritic cells (DC), neutrophils (N), mast cells (MC) and eosinophils (Eo) ($n = 5$ each). B, Using CNSortR, *Nf1*-OPGs and *Nf1*-R618X-OPGs contained mostly astrocytes (A) and oligodendrocytes (O), but also neurons (Ne), microglia (Mg), macrophages and monocytes, $CD8^+$ T cells, $CD4^+$ T cells, NK cells, plasma cells (PC), B cells, DCs, mast cells, endothelial cells (En), neutrophils, and eosinophils. C, Using scRNAseq, most populations matched those identified using

cells calculated by manual counting. Optic nerve sections were deparaffinized, hydrated and stained in toluidine blue (1% toluidine blue in 70% ethanol; pH 2.3) for 3 minutes, washed in distilled water, dehydrated, and mounted. Stained optic nerves were imaged for quantification on a Leica ICC50W microscope using LAS EZ software.

Immunofluorescence

Nf1-OPG optic nerves sections were prepared as above and incubated with appropriate primary and Alexa Fluor secondary antibodies (Supplementary Table S1).

ELISA

Active RAS (RAS-GTP; Fisher Scientific, 50673628), Ccl2 (Fisher Scientific, MJE00B), and Ccl5 (Fisher Scientific, MMR00) ELISAs were performed per manufacturers' instructions.

RNA Extraction, cDNA Production, and qPCR

RNA from mouse optic nerves and spleens was isolated using the NucleoSpin® RNA Plus kit (NC1498148, Takara), reverse transcribed into cDNA using the Applied Biosystems High-Capacity cDNA Reverse Transcription Kit (Thermo- 4374967), and subjected to TaqMan real-time quantitative PCR (RT-qPCR) (Supplementary Table S2). ΔΔCT values were calculated using *Gapdh* expression as an internal control.

T Cell Isolation

Mouse spleens were homogenized into single-cell suspensions in PBS containing 0.1% BSA and 0.6% Na-citrate, followed by 15 min incubation with 120 Kunitz units of DNase I, and erythrocyte lysis (eBioscience, 00433357). Cells were then filtered through a 30-μM cell strainer. $CD8^+$ and $CD4^+$T cells were isolated using CD8a (Miltenyi Biotec, 130-104-075) and CD4 (Miltenyi Biotec, 130-117-043) T cell isolation kits, respectively. T cells were grown at 2.5 x 10^6 cells/ml in RPMI-1640 medium supplemented with 10% FBS and 1% P/S. After 24h, *Nf1*+/- $CD8^+$T cells were treated for 24 h with 10 μM Pan-RAS-Inhibitor-IN-1 (IN-1[HY-101295, MedChem Express]) or 10 μM Ccr4 inhibitor (AZD2098, Selleckchem). All experiments were performed with $n = 3$.

Migration Assays

About 5 × 10^5 T cells were placed in the upper transwell chambers (Corning, 6.5 mm insert, CLS3398-2EA) containing 200 μl serum-free RPMI 1640 media. 500 μl of chemoattractant media containing Ccl2 (20ng/ml, 479-JE-050/CF-R&D systems) or Ccl12 (25ng/ml, 428-P5-025-R&D systems) was added to the lower chamber[11], and the number of T cells in the lower chambers counted by microscopy at 20x after 6 h.

Proliferation Assay

T cell proliferation was assessed using the BrdU Cell Proliferation ELISA Kit (Ab126556, Abcam) following the manufacturer's instructions. Briefly, 5 × 10^5 cells were plated in a 96-well plate and incubated for 72 h prior to the addition of BrdU for 24 h. Cells were then fixed, permeabilized, and subjected to DNA denaturation. Following incubation with anti-BrdU antibodies for 4 h, the cells were washed and incubated with peroxidase-conjugated secondary antibody, and analyzed using a colorimetric assay at 450nm.

Statistical Analyses

Data analyses were performed using GraphPad Prism using unpaired two-tailed Student's t-tests (differences between two groups) and one-way or two-way analysis of variance (ANOVA) with Dunnett's or Tukey's multiple comparisons test, with significance set at $p<0.05$. Data are presented as mean values ± SEM. All experiments were performed at least thrice with similar results, and statistical analyses verified by a bioinformatician (O.C.).

Results

The *Nf1*-OPG Microenvironment Contains Mostly T Cells and Microglia

To determine the non-neoplastic cell composition of murine *Nf1*-OPGs, we analyzed bulk tumor RNAseq data from two models of *Nf1*-OPG (*Nf1*-OPG, Figure 1A, left; *Nf1*-R681X-OPG; Figure 1A, right; GSE102345) at 12 WOA when >95% of the mice harbor tumors. Using TIMER 2.0, we found B cells, plasma cells, dendritic cells, NK cells, and mast cells, in addition to monocytes and T cells ($CD8^+$ and $CD4^+$ cells). Similarly, human PAs (NF1-associated and sporadic) contained B cells, plasma cells, macrophages, T cells, NK cells, dendritic cells, neutrophils, mast cells, and eosinophils (Supplementary Figure S1B).

Since TIMER was constructed using RNAseq data from peripheral immune cells, we amended ImmuCC with data from the *brainrnaseq.org*[19] to provide a better representation of the brain populations in murine *Nf1*-OPGs (CNSortR

CNSortR. D, No mast cells (toluidine blue), B cells (CD138), dendritic cells (dendritic cell receptor-2), or plasma cells (CD94) were detected in the optic nerves of control (CTL) or *Nf1*-OPG mice. E, Increased microglia ($Iba1^+$ cells), endothelial cells ($VCAM1^+$ cells), astrocytes ($GFAP^+$ cells), and oligodendrocytes/oligodendrocyte precursor cells ($Olig2^+$ cells), as well as greater $CD8^+$ and $CD4^+$ T cell content, were detected in the optic nerves of *Nf1*-OPG mice relative to controls (CTL). F, Nearly all $Iba1^+$ cells were $Tmem119^+$ cells (microglia) at all ages examined. Scale bar, 50 μm.

v.1.0). With the inclusion of neural cell types, we found predominantly oligodendrocytes and astrocytes (GSE102345, Figure 1B).

Next, scRNAseq of optic nerves from *Nf1*-OPG mice (n = 8) at 12 WOA identified 12 cell populations (Figure 1C, upper), including endothelial cells, mast cells, neutrophils, B cells, T cells, microglia, oligodendrocytes, and brain cells (astrocytes, neurons). To compare these to those detected by deconvolution analysis, we used the top 20 differentially expressed genes from each of the scRNAseq clusters, and matched them with the genes expressed in the CNSortR populations (Figure 1C). While most populations aligned well, with minor differences, all methods indicated that *Nf1*-OPGs contain mast cells, plasma cells, B cells, dendritic cells, and natural killer (NK) cells.

To determine whether these newly-identified cells were actually present in *Nf1*-OPGs, we performed immunostaining of optic nerves from CTL and *Nf1*-OPG mice at 12 WOA using established antibody markers for each population. Contrary to the bulk RNA-seq deconvolution and scRNAseq results, no mast cells (Toluidine blue-positive), B cells (CD19$^+$), dendritic cells (Dendritic Cell Inhibitory Receptor 2$^+$), plasma cells (CD138$^+$) or NK cells (CD94$^+$) were detected in any of the murine optic nerves (Figure 1D), in normal human brain (n = 26) or in patient PA tissue specimens (n = 67; Supplementary Figure S1C). In contrast, we found that *Nf1*-OPG mouse tumors contained monocytes (Iba1$^+$ cells), endothelial cells (VCAM1$^+$ cells), astrocytes (GFAP$^+$ cells), and oligodendrocyte precursors/oligodendrocytes (Olig2$^+$ cells), as well as CD8$^+$ and CD4$^+$ T cells (Figure 1E). We also observed that the T cells identified in murine *Nf1*-OPG tumors at 12 WOA were sometimes, but not always, adjacent to VCAM-1$^+$ blood vessels (Supplementary Figure S1D).

Since RNAseq data from peripheral immune cells may not accurately identify the analogous populations in the brain, we hypothesized that the RNAseq markers defining those populations (BAFF-R, B cells; TPSB2, mast cells) might be expressed by another population. As such, BAFF-R is largely expressed by Iba1$^+$ monocytes (macrophages/microglia) in the *Nf1*-OPG optic nerves, whereas TPSB2 was mostly found in GFAP$^+$ cells (astrocytes) (Supplementary Figure S1E). Since Iba1 is not a specific marker for microglia, and also identifies other monocyte populations, we sought to determine what proportion of the Iba1$^+$ cells were microglia. Using Tmem119 as a marker of microglia[25], nearly all of the Iba1$^+$ cells were Tmem119$^+$ (Figure 1F).

Murine *Nf1*-OPG Growth Begins After 6 Weeks of Age

Since the majority of optic nerve myelination occurs postnatally[26], we assessed proliferation in the optic nerves of WT, *Nf1+/–*, and *Nf1*-OPG mice at 3, 4.5, 6, 9, and 12 WOA (Figure 2A). While both non-tumor-forming (WT, *Nf1+/–*) and tumor-forming (*Nf1*-OPG) mouse optic nerves had high levels of proliferation at 3 WOA, this increased proliferation was reduced in non-tumor-forming mice by 6 WOA. Conversely, tumor-forming (*Nf1*-OPG) optic nerves increased their proliferation over time. As expected, almost all proliferating cells at 3 and 6 WOA in all mice were Olig2$^+$ oligodendroglial lineage cells (Figure 2B), demonstrating that *Nf1*-OPG development begins after 6 WOA when normal oligodendrocyte precursor cell proliferation declines to 20% (Figure 2C). At 12 weeks of age, the majority of the proliferating cells are CD133$^+$ and ABCG1$^+$ glioma cells[27,28] (Figure 2C), but not CD3$^+$ T cells or Tmem119$^+$ microglia.

Microglia and T Cells Exhibit Different Patterns of Temporal Evolution

To define the kinetics of microglia expansion and Ccl5 production, we analyzed optic nerves from control (WT or *Nf1*$^{flox/flox}$), *Nf1+/–*, and *Nf1*-OPG mice beginning at 3 WOA, before tumors developed[15], as well as at 4.5, 6, and 9 (tumor evolution) and 12 (fully formed tumors) WOA. While Tmem119$^+$ microglia content was similar in all groups at 3 and 4.5 WOA, Tmem119$^+$ microglia increased in *Nf1*-OPG mice at 6 WOA relative to control (WT) and *Nf1+/-* mice (Figure 3A). Importantly, Iba1$^+$ (Supplementary Figure S2A) and CD11b$^+$ microglia (Supplementary Figure S2B) exhibit similar patterns to the Tmem119$^+$ microglia profiles (Figure 3B). At 6 WOA, in parallel with increased microglia content, Ccl5 expression increased (Figure 3C) in *Nf1*-OPG relative to WT mice. Relevant to human LGGs, *CCL5* RNA expression was increased in sporadic and NF1-associated pediatric PAs relative to non-neoplastic brain in two independent GEO datasets (Figure 3D–E).

Next, we analyzed the temporal dynamics of optic nerve T cell infiltration in WT, *Nf1+/–*, and *Nf1*-OPG mice at 3, 4.5, 6, 9, and 12 WOA (Figure 4A). CD3$^+$ T cell content begins to rise exclusively in *Nf1*-OPG mice after 9 WOA. Since we had previously shown that Ccl2 mediates T cell infiltration into the optic nerves of *Nf1*-OPG mice[11], we quantified Ccl2 expression as a function of tumor evolution, and found that Ccl2 expression increases after 6 WOA in *Nf1*-OPG mice (Figure 4B). Additionally, *CCL2* expression was increased in sporadic and NF1-associated pediatric PAs relative to non-neoplastic brain in two independent GEO datasets (Figure 4C–D).

CD8$^+$T Cell Predominance is Governed by NF1/RAS Regulation of Ccr4 Expression

The majority of the tumor-infiltrating T cells were CD8$^+$ T lymphocytes (Figure 5A), as previously reported in mice[13] and in human NF1-LGGs[8]. In contrast, the number of CD4$^+$ T cells was similar in tumor-bearing (*Nf1*-OPG) and nontumor-bearing (WT, *Nf1+/–*) optic nerves from 3 to 12 WOA (Figure 5B). Importantly, the sum of the CD4$^+$ and CD8$^+$T cells in the optic nerves equaled the total number of CD3$^+$ T cells (Supplementary Figure S3A), suggesting that these are the major T cell populations in murine *Nf1*-OPGs. No regulatory (Foxp3$^+$), helper (CD25$^+$), or exhausted T (PD-1$^+$ or Lag3$^+$) cells were detected in these tumors at any time point (Supplementary Figure S3B).

To determine the etiologic basis for the selective recruitment of CD8$^+$T cells, we examined directed migration

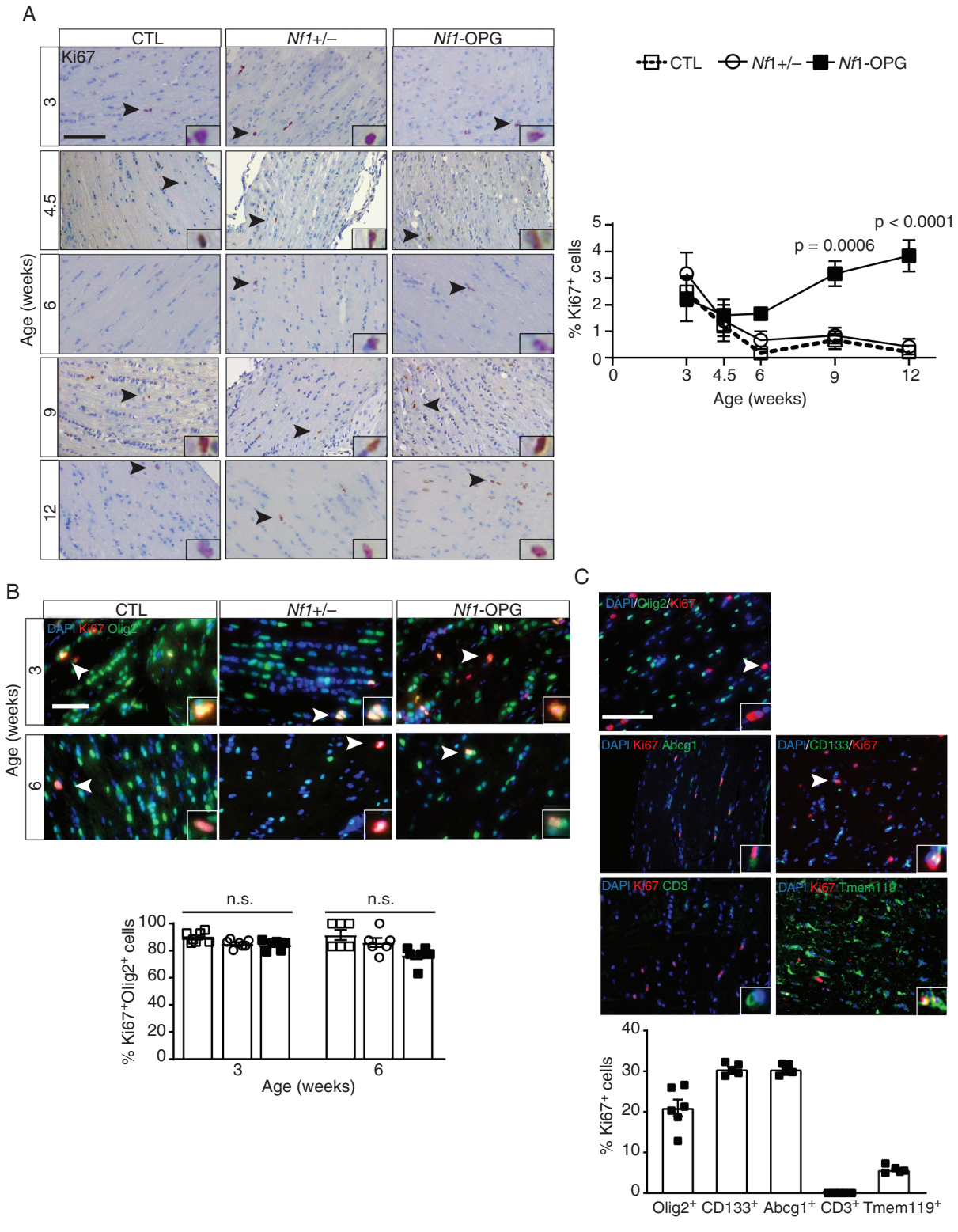

Figure 2. Optic glioma proliferation begins after 6 weeks of age. A, No difference in proliferation (%Ki67$^+$ cells) in the optic nerves of CTL ($n = 6$), *Nf1*+/– ($n = 6$), and *Nf1*-OPG ($n = 5$) were noted at 3, 4.5, or 6 WOA. At 9 and 12 WOA, *Nf1*-OPG mice have more Ki67$^+$ cells compared to CTL and *Nf1*+/– mice ($P = 0.006$ and $P < 0.001$, respectively). B, At 3 ($n = 7$ per group) and 6 ($n = 6$ per group) WOA, most Ki67$^+$ cells were Olig2$^+$ cells in all optic nerves. C, At 12 WOA, the majority of the Ki67$^+$ cells in the murine *Nf1*-OPGs were Olig2$^+$ cells or CD133$^+$ and ABCG1$^+$ glioma cells.

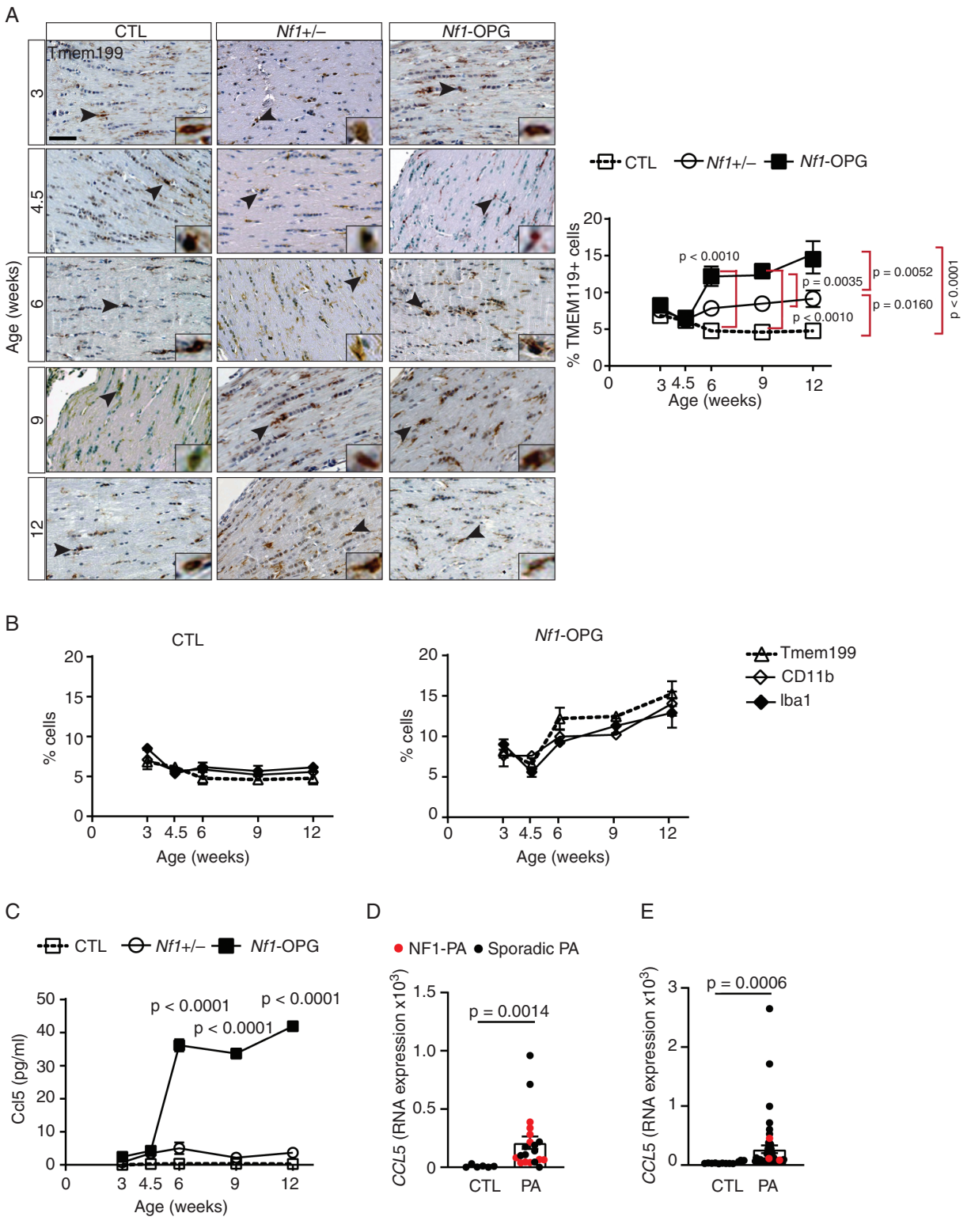

Figure 3. *Nf1*-OPG microglia content and Ccl5 production increase by 6 weeks of age. A, Similar Tmem119$^+$ cell content in the optic nerves of all mice were noted at 3 WOA. *Nf1*-OPG mice ($n = 5$) have more Tmem119$^+$ cells at 6 and 9 weeks compared to both *Nf1*+/– and CTL mice (both $n = 6$, $P = 0.0029$). At 12 WOA, CTL mice have the lowest density of microglia. *Nf1*-OPG ($P < 0.0001$) and *Nf1*+/– ($P = 0.006$) optic nerves have more microglia relative to controls. B, No differences in Iba1$^+$, Tmem119$^+$ and CD11b$^+$ cell content were observed between control and *Nf1*-OPG mice. C, Higher Ccl5 levels were detected in the optic nerves of 6- ($P < 0.0001$), 9- ($P < 0.0001$) and 12- ($P < 0.0001$) week-old *Nf1*-OPG mice, but not in 3-week-old mice, relative to controls ($n = 3$ all). Human PAs have increased *CCL5* expression by D, RNAseq and E, microarray relative to non-neoplastic brain (CTL). Scale bar, 50 μm.

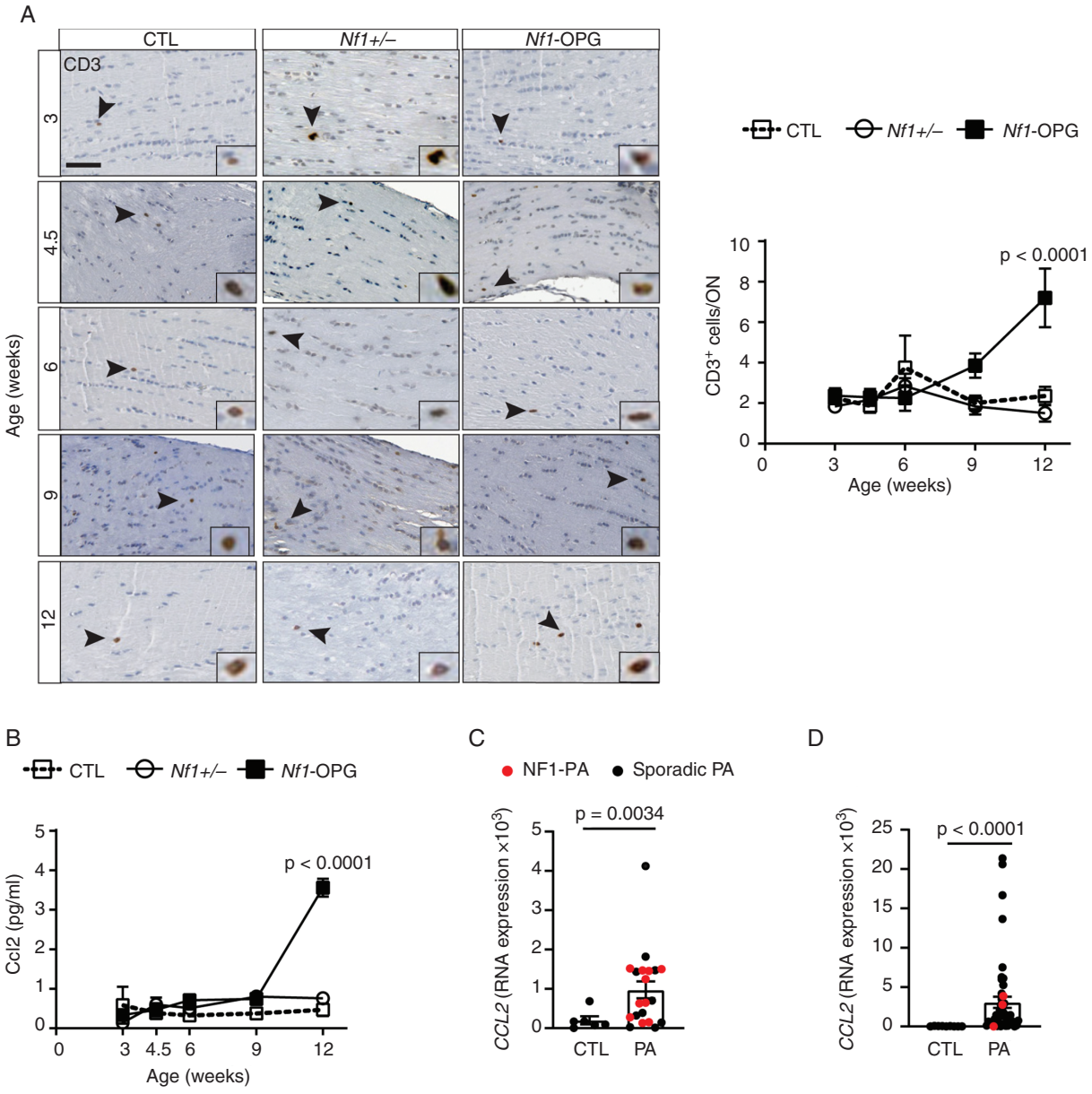

Figure 4. *Nf1*-OPG T cells and Ccl2 levels rise after 6 weeks of age. A, *Nf1*-OPG ($n = 5$) CD3⁺ T cells infiltrate after 9 WOA ($P < 0.0001$). There was no difference in CD3⁺ T cells between CTL and *Nf1*-OPG mice (both $n = 6$) at 3, 4.5, 6, and 9 WOA. *Nf1*+/– mice have similar CD3⁺ T cell content as controls at 3, 4.5, 6, 9, and 12 WOA. B, Ccl2 levels are similar to CTL mice at 3, 4.5, 6 and 9 WOA, but increase by 12 WOA in *Nf1*-OPG mice compared to controls ($n = 3$ all, $P < 0.0001$). Human PAs have increased *CCL2* expression by C, RNAseq and D, microarray relative to non-neoplastic brain (CTL). Scale bar, 50 μm.

of CD4⁺ and CD8⁺ T cells to Ccl2 and Ccl12, chemokines secreted by neoplastic cells to mediate T cell migration[11]. While *Nf1+/–* and WT CD4⁺ T cell migration to Ccl2 and Ccl12 were similar, *Nf1+/–* CD8⁺ T cells had greater migration to Ccl2, but not Ccl12, than their WT counterparts (Figure 5C). One plausible explanation for the increased directed migration of CD8⁺ T cells to Ccl2 is differential expression of Ccl2 receptors (Ccr2 and Ccr4). Using RT-qPCR, we detected increased *Ccr4* expression in *Nf1+/-* CD8⁺ T cells relative to WT CD8⁺, CD4⁺ T cells, and *Nf1+/–* CD4⁺ T cells (Figure 5D), without any change in *Ccr2* expression (Supplementary Figure S3C). Similar increases in *Ccr4* expression were observed in CD8⁺ T cells from other *Nf1*-OPG strains (R681X and R1278P) relative to their WT counterparts (Supplementary Figure S3D). Consistent with Ccr4 as the receptor responsible for increased *Nf1+/–* CD8⁺ T cell Ccl2-directed migration, treatment of *Nf1+/–* CD8⁺ T cells with a selective Ccr4 inhibitor (AZD2098) reduced the migration of *Nf1+/–* CD8⁺ T cells to Ccl2, but not Ccl12 (Figure 5E).

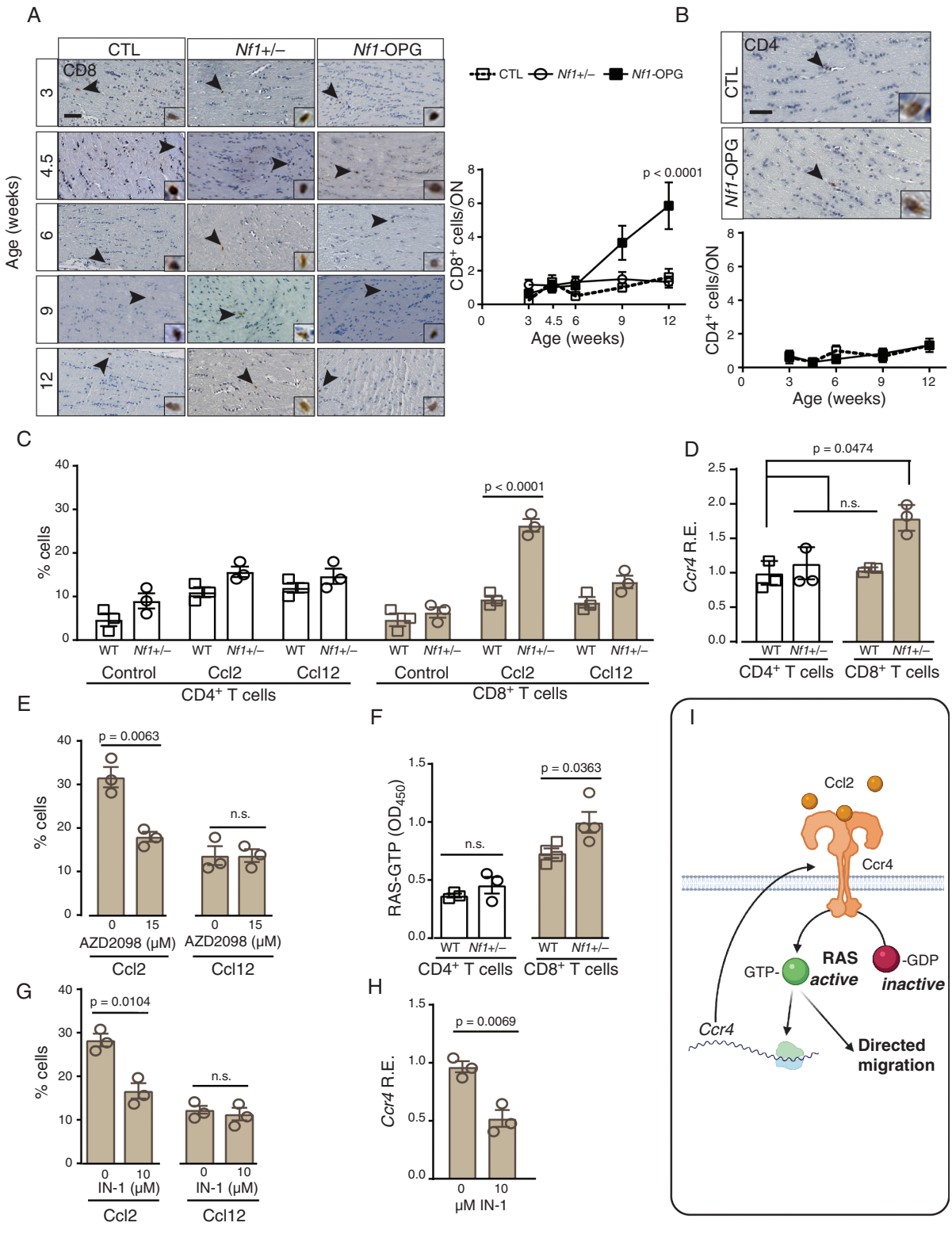

Figure 5. CD8+T cell predominance is governed by NF1/RAS regulation of Ccr4 expression. A, $CD8^+$ T cells content in *Nf1*-OPG optic nerves ($n = 10$) is similar to controls ($n = 8$) at 3, 4.5, 6, and 9 WOA, but increases by 12 WOA ($P < 0.0001$). *Nf1*+/– mice ($n = 6$) have similar numbers of $CD8^+$ T cells as controls from 3 to 12 WOA. B, $CD4^+$ T cell content does not change in *Nf1*-OPG optic nerves relative to controls at 3, 4.5, 6, 9, and 12 WOA. C, Ccl2 did not increase $CD4^+$ T cell migration in WT or *Nf1*+/– mice. Ccl12 or medium (control) does not increase $CD4^+$ T cell migration. Ccl2 increased *Nf1*+/– $CD8^+$ T cell migration relative to WT controls ($P < 0.0001$). *Nf1*+/- and WT $CD8^+$ T cells treated with medium (Control) or Ccl12 exhibit similar

One of the consequences of increased Ccr4 activation in *Nf1+/–* CD8+ T cells is elevated RAS activity. To this end, WT CD8+ T cells have higher levels of RAS activity than WT CD4+ cells, which is further increased in the setting of an *Nf1* mutation (*Nf1+/–* T cells; Figure 5F). Consistent with NF1/RAS regulation of migration, inhibition of RAS activity (IN-1) decreased CD8+ T cell migration to Ccl2, but not Ccl12, with no effects on CD4+ T cell migration (Figure 5G). Since the increase in *Ccr4* expression was larger than the increase in RAS activity detected in CD8+ T cells, we sought to determine whether RAS activation regulates *Ccr4* expression. Consistent with a feed-forward loop where *Nf1* mutation leads to greater RAS activity and *Ccr4* expression, IN-1 treatment reduced *Ccr4* expression in *Nf1+/–* CD8+ T cells (Figure 5H-I). In addition to increased Ccl2-mediated chemotaxis, *Nf1+/–* CD8+ T cells exhibited greater proliferation than their WT counterparts (Supplementary Figure S3E).

Interrupting T Cell and Microglia Function During Tumor Formation Blocks *Nf1*-OPG Progression

Leveraging the unique temporal patterns of microglia and T cell infiltration, we performed three proof-of-principle experiments to determine whether blocking these events during the specific time intervals would abrogate glioma progression. Since microglia content and Ccl5 production begin to increase after 3 WOA, we first treated *Nf1*-OPG mice with the PLX3397 inhibitor from 4-7 WOA to deplete microglia, and analyzed the optic nerves at 6 months of age. While there were fewer microglia and CD3+ T cells (Supplementary Figure S4), optic nerve proliferation (Ki67+ cells) was unchanged, suggesting that depleting microglia was insufficient to block tumor development.

Second, *Nf1*-OPG mice were treated with anti-Ccl5 antibodies from 3 to 6 WOA, when Ccl5 expression rises, and aged to 12 WOA when *Nf1*-OPG become evident. Compared to control antibody-treated mice, *Nf1*-OPG mice treated with anti-Ccl5 antibodies had reduced proliferation, without changes in microglia content (Figure 6A) or optic nerve volume (Figure 6B). Importantly, the lack of tumor proliferation was associated with reduced *Ccl2* expression (Figure 6C) and Ccl2-mediated T cell infiltration (Figure 6A). After aging a separate cohort of anti-Ccl5 antibody-treated mice to 6 months of age, the decrease in proliferation and infiltration of T cells persisted (Figure 6D).

Third, we treated *Nf1*-OPG mice with anti-Ccl2 antibodies from 7 to 10 WOA, when Ccl2 expression and Ccl2-mediated CD8+ T cell infiltration increase. Relative to mice receiving control antibodies, *Nf1*-OPG mice treated with anti-Ccl2 antibodies had reduced tumor proliferation (Ki67+), CD3+ T cell content, and Ccl5 production, with no change in microglia content or optic nerve volume (Figure 6E–G). The reduced proliferation and T cell infiltration seen at 12 WOA remained when a separate cohort of mice were analyzed at 6 months of age (Figure 6H).

Discussion

Stromal dependence is a hallmark of most solid cancers, including brain tumors, where its importance to tumor formation and progression has been mainly explored in malignant gliomas[29–39]. In the current study, we employed *Nf1*-mutant mouse strains to characterize the LGG immune microenvironment composition, define the temporal sequence of tumor evolution, and use this information to identify therapeutic windows to block glioma progression. Herein, we show that durable inhibition of gliomagenesis is achieved by interrupting Ccl2-mediated T cell infiltration or microglia production of Ccl5. Moreover, we demonstrate that selective CD8+ T cell enrichment in these tumors results from NF1/RAS-regulated *Ccr4* expression. Collectively, these findings raise three major points relative to LGG pathobiology.

First, we show that disrupting stromal cell function during critical periods of tumor formation is sufficient to block tumorigenesis. In this manner, we show that anti-Ccl2 antibody-mediated interruption of T cell infiltration and anti-Ccl5 antibody-mediated abrogation of glioma cell microenvironmental support reduces *Nf1*-OPG proliferation, one key hallmark of these tumors in children. However, microglia content and optic nerve volumes are not restored to WT levels. We interpret this result to indicate that disrupting the stromal axis during tumor evolution blocks *Nf1*-OPG progression, but does not abrogate glioma initiation. In this manner, the events required for tumor initiation have already occurred, such that these treatments merely block further evolution of the tumor, ameliorating its growth (%Ki67+ cells), but not the microglia infiltration or optic nerve volume. To this end, observations from our laboratory have revealed that *Nf1+/-* mice have increased optic nerve volumes and microglia content, similar to some children with NF1[40], arguing that these stroma-directed treatments do not completely normalize the NF1-associated optic nerve pathology. In contrast, we have previously shown that *Nf1*-OPG initiation is dictated by retinal ganglion cell neuronal activity-dependent production of neuroligin-3 (NGLN3)[41]. Taken together, we envision gliomagenesis involves at least three separable epochs: (1) initiation, reflecting the impact of *Nf1* mutation on the cells of origin for these tumors[42] or on neuronal activity-regulated Nlgn3 production, (2) propagation, which entails T cell recruitment and elaboration of microglia-produced gliomagens (*e.g.*, Ccl5), and/or (3) maintenance involving some of the same signals and cell types.

migration. D, *Nf1*+/- and WT CD4+ T cells had similar levels of *Ccr4* expression. *Nf1*+/– CD8+ T cells have increased *Ccr4* expression relative to their WT counterparts ($P = 0.0474$). E, Ccr4 inhibition (AZD2098; 15μM) in CD8+ T cells decreases Ccl2-induced, but not Ccl12-induced, migration ($P = 0.0063$). F, *Nf1*+/– and WT CD4+ T cells had similar levels of Ras activity. *Nf1*+/– CD8+ T cells have increased Ras activity relative to their WT counterparts ($P = 0.0363$) G, Inhibition of Ras activity (10μM IN-1) reduces Ccl2-induced,but not Ccl12-induced, CD8+ T cell migration ($P = 0.0104$). H, RAS activity inhibition (10μM IN-1) decreases *Ccr4* expression in *Nf1+/-* CD8+ T cells ($P = 0.0069$). I, Proposed model of Ccl2 signaling through Ccr4 in *Nf1+/–* CD8+ T cells.

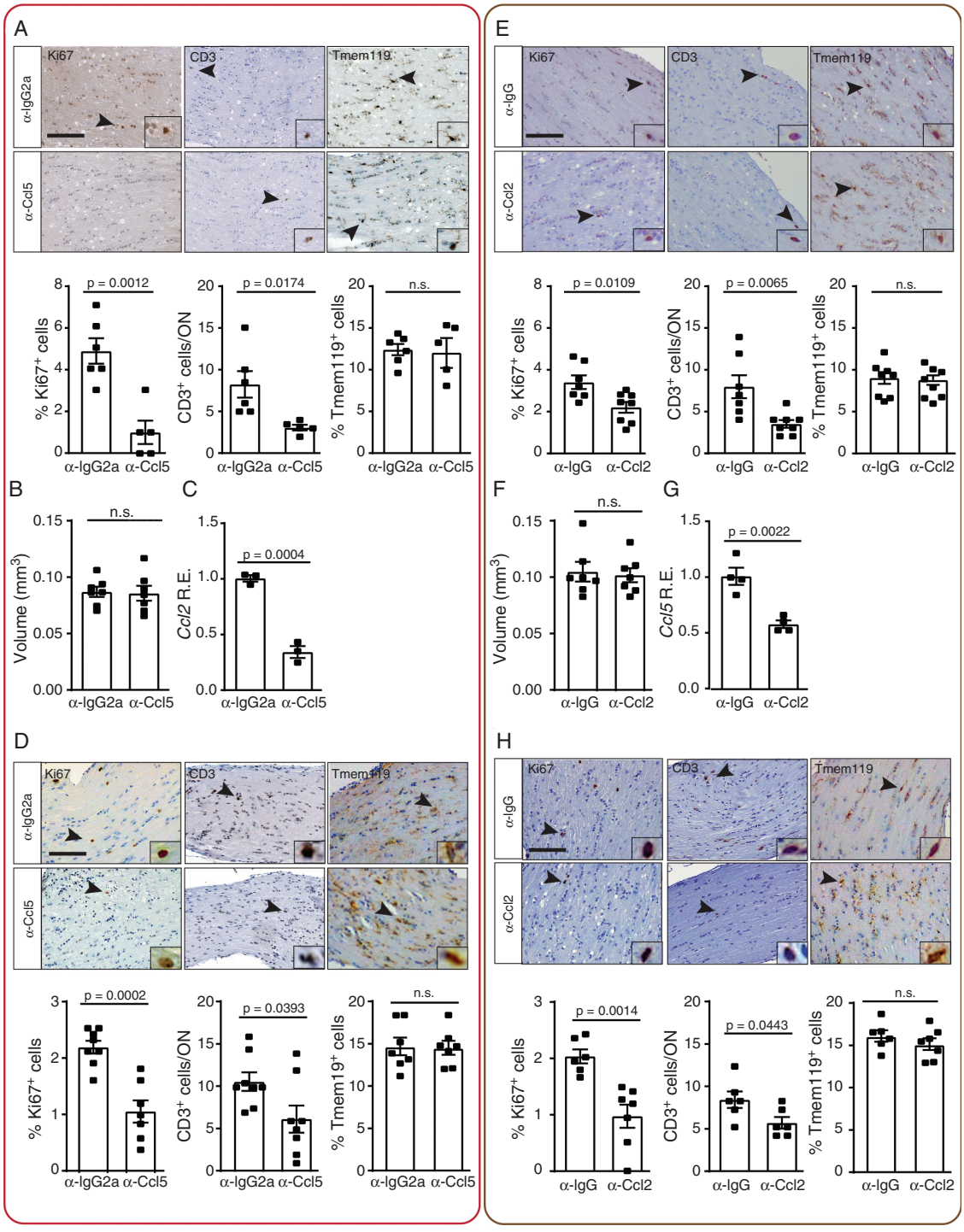

Figure 6. Interrupting microglia or T cell function during tumor evolution blocks *Nf1*-OPG progression. A, Ccl5 neutralizing antibody ($n = 5$) treatment (3 to 6 WOA) results in decreased *Nf1*-OPG proliferation (%Ki67$^+$ cells; $P = 0.0012$) and CD3$^+$ T cells content relative to anti-IgG2a isotype controls ($n = 6$, $P = 0.0174$). No difference in microglia content was found between both groups. B, No difference in the volumes of the optic nerves were observed between anti-Ccl5- and anti-IgG2a-treated mice. C, *Nf1*-OPG mice treated with anti-Ccl5 neutralizing antibodies had reduced *Ccl2* expression ($P = 0.0004$) relative to isotype control-treated mice (both $n = 3$). D, At 24 WOA, anti-Ccl5-treated mice (3 to 6 WOA) had decreased proliferation (%Ki67$^+$ cells; $P = 0.0002$) and CD3$^+$ T cell content ($P = 0.0393$) compared to anti-IgG-treated mice. E, Anti-Ccl2 neutralizing antibody treatment ($n = 8$, 7 to 10 WOA) resulted in decreased proliferation (%Ki67$^+$ cells; $P = 0.0109$) and decreased CD3$^+$ T cell infiltration ($P = 0.0065$). No difference in microglia content was seen between anti-Ccl2- and anti-IgG-treated ($n = 7$) mice. F, No differences in optic nerve volumes were observed between both groups. G, Anti-Ccl2 antibody treatment reduced optic nerve *Ccl5* levels ($P = 0.0022$) compared to IgG-treated mice. H, At 24 WOA, anti-Ccl2-treated mice (7 to 10 WOA) had decreased proliferation (%Ki67$^+$ cells; $P = 0.0014$) and CD3$^+$ T cell content ($P = 0.0443$) relative to IgG-treated mice.

Second, prior studies in *Nf1*-OPG mice[11,13] and NF1 patient gliomas[8] revealed a striking predominance of CD8+ T cells. We previously demonstrated that neoplastic cell-produced Ccl2 (which signals through both Ccr2 and CCr4 receptors) and Ccl12 (which signals through Ccr2 receptor) are responsible for T cell-directed migration[11]. Surprisingly, *Nf1* mutation increases RAS activation, proliferation, and Ccl2-mediated migration more dramatically in CD8+ T cells, where it selectively increases *Ccr4* RNA expression in a RAS-dependent manner. Moreover, the increased *Ccr4* expression is likely responsible for the increased CD8+ T cell content observed in *NF1*-mutant tumors, as further supported by increased *Ccr4* expression in CD8+ T cells from mice harboring different germline *Nf1* gene mutations (Supplementary Figure S3D) and inhibition of T cell motility in response to Ccl2. Additional studies are underway to determine why RAS is selectively hyperactivated in *Nf1+/–* CD8+ T cells, and how this RAS/Ccr4 feedforward loop is maintained.

While CD8+ T cells are increased in the tumors and are critical for glioma proliferation[13], it is not clear whether they are exhausted[43,44] or dysfunctional[45] CD8+ T cells or a unique population of T cells that promote microglia support of tumor cell growth. Analysis of these lymphocytes reveals that they do not express CD94 (NK cells), PD-1 (exhausted T cells) or Foxp3/CD25 (T helper cells). While further characterization of *Nf1*-OPG CD8+ T cells is necessary, a population of innate CD8+ T cells that do not recognize classic peptide antigens has been reported to promote tumorigenesis[46].

Third, these findings support the need for further research into stroma-directed therapies. While microglia inhibitors, like PLX3397 (CSF1R targeting), were promising in preclinical studies[47,48], they only transiently deplete microglia, and had limited efficacy in a phase II clinical trial[49]. Similarly, PLX3397 treatment of *Nf1*-OPG mice from 4 to 7 WOA had no durable effect on tumor growth when assayed at 25 WOA, despite a persistent reduction in microglia content. In contrast, interrupting the T cell/microglia immune axis resulted in durable effects, with mice exhibiting reduced glioma proliferation >3 months after the cessation of treatment. Taken together, these data reveal critical windows of tumor evolution during which stromal targeting abrogates glioma progression. Moreover, the ability to inhibit the supportive tumor microenvironment for a short period of time is particularly attractive for the treatment of pediatric LGGs that arise in the context of a developing brain.

Supplementary material

Supplemental material is available at *Neuro-Oncology Advances* online.

Keywords

chemokines | low-grade glioma | microglia | T cells | tumor microenvironment.

Funding

This work was funded by grants from the National Institutes of Health (1-R35-NS07211-01 to D.H.G., Alex's Lemonade Stand Foundation (POST Award) 5-T35-HL007815 to E.C., P30EY002687, S10 RR0227552) and Gilbert Family Foundation (Vision Restoration Initiative; #600495), The Genome Technology Access Center is partially supported by grants from the NCI (#P30 CA91842, UL1TR002345). The Washington University Ophthalmology Core facility support is supported by funding from the National Eye Institute (P30EY002687).

Conflict of interest. D.H.G. has a licensing agreement for the use of GFAP-Cre mice. The other authors disclosure no relevant conflicts of interest.

Authorship statement. D.H.G., A.A.C. and J.C. designed the experiments and wrote the manuscript drafts. A.A.C. prepared the figures, and D.H.G. edited the manuscript. A.A.C. and J.C. performed the experiments and analyzed the results, with assistance from E.C., S.S., A.C. and A.G. O.C. performed the bioinformatics analysis. S.D. provided the human samples. D.H.G. provided funding.

References

1. Patil N, Kelly ME, Yeboa DN, et al. Epidemiology of brainstem high-grade gliomas in children and adolescents in the United States, 2000–2017. *Neuro-Oncology* 2021;23(6):990–998.
2. Fisher MJ, Jones DTW, Li Y, et al. Integrated molecular and clinical analysis of low-grade gliomas in children with neurofibromatosis type 1 (NF1). *Acta Neuropathol* 2021; 141(4):605–617.
3. de Blank PMK, Fisher MJ, Liu GT, et al. Optic pathway gliomas in neurofibromatosis type 1: an update: surveillance, treatment indications, and biomarkers of vision. *J Neuro-Ophthalmol* 2017; 37(Suppl 1):S23–S32.
4. Yuan M, White D, Resar L, et al. Conditional reprogramming culture conditions facilitate growth of lower-grade glioma models. *Neuro-Oncology* 2021; 23(5):770–782.
5. Raabe EH, Lim KS, Kim JM, et al. BRAF activation induces transformation and then senescence in human neural stem cells: a pilocytic astrocytoma model. *Clin Cancer Res* 2011; 17(11):3590–3599.
6. Buhl JL, Selt F, Hielscher T, et al. The senescence-associated secretory phenotype mediates oncogene-induced senescence in pediatric pilocytic astrocytoma. *Clin Cancer Res* 2019; 25(6):1851–1866.
7. Jacob K, Quang-Khuong DA, Jones DT, et al. Genetic aberrations leading to MAPK pathway activation mediate oncogene-induced senescence in sporadic pilocytic astrocytomas. *Clin Cancer Res* 2011; 17(14):4650–4660.
8. D'Angelo F, Ceccarelli M, Tala, et al. The molecular landscape of glioma in patients with Neurofibromatosis 1. *Nat Med* 2019; 25(1):176–187.

9. Bajenaru ML, Hernandez MR, Perry A, et al. Optic nerve glioma in mice requires astrocyte Nf1 gene inactivation and Nf1 brain heterozygosity. *Cancer Res* 2003; 63(24):8573–8577.
10. Hegedus B, Banerjee D, Yeh TH, et al. Preclinical cancer therapy in a mouse model of neurofibromatosis-1 optic glioma. *Cancer Res* 2008; 68(5):1520–1528.
11. Guo X, Pan Y, Gutmann DH, Genetic and genomic alterations differentially dictate low-grade glioma growth through cancer stem cell-specific chemokine recruitment of T cells and microglia. *Neuro-Oncology* 2019; 21(10):1250–1262.
12. Pan Y, Xiong M, Chen R, et al. Athymic mice reveal a requirement for T-cell-microglia interactions in establishing a microenvironment supportive of Nf1 low-grade glioma growth. *Genes Develop* 2018; 32(7–8):491–496.
13. Guo X, Pan Y, Xiong M, et al. Midkine activation of CD8(+) T cells establishes a neuron-immune-cancer axis responsible for low-grade glioma growth. *Nat Commun* 2020; 11(1):2177.
14. Solga AC, Pong WW, Kim KY, et al. RNA sequencing of tumor-associated microglia reveals Ccl5 as a stromal chemokine critical for neurofibromatosis-1 glioma growth. *Neoplasia* 2015; 17(10):776–788.
15. Toonen JA, Ma Y, Gutmann DH, Defining the temporal course of murine neurofibromatosis-1 optic gliomagenesis reveals a therapeutic window to attenuate retinal dysfunction. *Neuro-Oncology* 2017; 19(6):808–819.
16. Brannan CI, Perkins AS, Vogel KS, et al. Targeted disruption of the neurofibromatosis type-1 gene leads to developmental abnormalities in heart and various neural crest-derived tissues. *Genes Develop* 1994; 8(9):1019–1029.
17. Toonen JA, Anastasaki C, Smithson LJ, et al. NF1 germline mutation differentially dictates optic glioma formation and growth in neurofibromatosis-1. *Hum Mol Genet* 2016; 25(9):1703–1713.
18. Partek Inc. Partek® Genomics Suite® (Version 7.0 Computer software). https://www.partek.com/partek-genomics-suite/ 2020.
19. Zhang Y, Chen K, Sloan SA, et al. An RNA-sequencing transcriptome and splicing database of glia, neurons, and vascular cells of the cerebral cortex. *J Neurosci* 2014; 34(36):11929–11947.
20. Dobin A, Davis CA, Schlesinger F, et al. STAR: ultrafast universal RNA-seq aligner. *Bioinformatics* 2013; 29(1):15–21.
21. Chen Z, Quan L, Huang A, et al. seq-ImmuCC: cell-centric view of tissue transcriptome measuring cellular compositions of immune microenvironment from mouse RNA-seq data. *Front Immunol* 2018; 9:1286.
22. Law CW, Chen Y, Shi W, Smyth GK, voom: Precision weights unlock linear model analysis tools for RNA-seq read counts. *Genome Biol* 2014; 15(2):1–17.
23. Newman AM, Steen CB, Liu CL, et al. Determining cell type abundance and expression from bulk tissues with digital cytometry. *Nat Biotechnol* 2019; 37(7):773–782.
24. Li T, Fu J, Zeng Z, et al. TIMER2. 0 for analysis of tumor-infiltrating immune cells. *Nucleic Acids Res* 2020; 48(W1):W509–W514.
25. Bennett ML, Bennett FC, Liddelow SA, et al. New tools for studying microglia in the mouse and human CNS. *Proc Natl Acad Sci USA* 2016; 113(12):E1738–1746.
26. Ono K, Hirahara Y, Gotoh H, et al. Origin of oligodendrocytes in the vertebrate optic nerve: a review. *Neurochem Res* 2018; 43(1):3–11.
27. Chen YH, Cimino PJ, Luo J, Dahiya S, Gutmann DH, ABCG1 maintains high-grade glioma survival in vitro and in vivo. *Oncotarget* 2016; 7(17):23416–23424.
28. Chen YH, McGowan LD, Cimino PJ, et al. Mouse low-grade gliomas contain cancer stem cells with unique molecular and functional properties. *Cell Rep* 2015; 10(11):1899–1912.
29. Herting CJ, Chen Z, Pitter KL, et al. Genetic driver mutations define the expression signature and microenvironmental composition of high-grade gliomas. *Glia* 2017; 65(12):1914–1926.
30. Klemm F, Maas RR, Bowman RL, et al. Interrogation of the microenvironmental landscape in brain tumors reveals disease-specific alterations of immune cells. *Cell* 2020; 181(7):1643–1660.e1617.
31. Wang Q, Hu B, Hu X, et al. Tumor evolution of glioma-intrinsic gene expression subtypes associates with immunological changes in the microenvironment. *Cancer Cell* 2017; 32(1):42–56.e46.
32. Catalano M, D'Alessandro G, Trettel F, Limatola C, Role of infiltrating microglia/macrophages in glioma. *Adv Exp Med Biol* 2020; 1202:281–298.
33. De Boeck A, Ahn BY, D'Mello C, et al. Glioma-derived IL-33 orchestrates an inflammatory brain tumor microenvironment that accelerates glioma progression. *Nat Commun* 2020; 11(1):4997.
34. Quail DF, Joyce JA, The microenvironmental landscape of brain tumors. *Cancer Cell* 2017; 31(3):326–341.
35. Sadahiro H, Kang KD, Gibson JT, et al. Activation of the receptor tyrosine kinase AXL regulates the immune microenvironment in glioblastoma. *Cancer Res* 2018; 78(11):3002–3013.
36. Segura-Collar B, Garranzo-Asensio M, Herranz B, et al. Tumor-derived pericytes driven by EGFR mutations govern the vascular and immune microenvironment of gliomas. *Cancer Res* 2021;81(8):2142–2156.
37. Takacs GP, Flores-Toro JA, Harrison JK, Modulation of the chemokine/chemokine receptor axis as a novel approach for glioma therapy. *Pharmacol Ther* 2020; 222:107790.
38. Takenaka MC, Gabriely G, Rothhammer V, et al. Control of tumor-associated macrophages and T cells in glioblastoma via AHR and CD39. *Nat Neurosci* 2019; 22(5):729–740.
39. Uneda A, Kurozumi K, Fujimura A, et al. Differentiated glioblastoma cells accelerate tumor progression by shaping the tumor microenvironment via CCN1-mediated macrophage infiltration. *Acta Neuropathol Commun* 2021; 9(1):29.
40. Chatterjee J, Sanapala S, Cobb O, et al. Asthma reduces glioma formation by T cell decorin-mediated inhibition of microglia. *Nat Commun* 2021;12(1):7122.
41. Pan Y, Hysinger JD, Barron T, et al. NF1 mutation drives neuronal activity-dependent initiation of optic glioma. *Nature* 2021; 594(7862):277–282.
42. Brossier NM, Thondapu S, Cobb OM, Dahiya S, Gutmann DH, Temporal, spatial, and genetic constraints contribute to the patterning and penetrance of murine neurofibromatosis-1 optic glioma. *Neuro-Oncology* 2021; 23(4):625–637.
43. Woroniecka K, Chongsathidkiet P, Rhodin K, et al. T-cell exhaustion signatures vary with tumor type and are severe in glioblastoma. *Clin Cancer Res* 2018; 24(17):4175–4186.
44. Nakashima H, Alayo QA, Penaloza-MacMaster P, et al. Modeling tumor immunity of mouse glioblastoma by exhausted CD8(+) T cells. *Sci Rep* 2018; 8(1):208.
45. Schietinger A, Philip M, Krisnawan VE, et al. Tumor-specific T cell dysfunction is a dynamic antigen-driven differentiation program initiated early during tumorigenesis. *Immunity* 2016; 45(2):389–401.
46. Yan J, Allen S, McDonald E, et al. MAIT cells promote tumor initiation, growth, and metastases via tumor MR1. *Cancer Discovery* 2020; 10(1):124–141.
47. Pyonteck SM, Akkari L, Schuhmacher AJ, et al. CSF-1R inhibition alters macrophage polarization and blocks glioma progression. *Nat Med* 2013; 19(10):1264–1272.
48. Yan D, Kowal J, Akkari L, et al. Inhibition of colony stimulating factor-1 receptor abrogates microenvironment-mediated therapeutic resistance in gliomas. *Oncogene* 2017; 36(43):6049–6058.
49. Butowski N, Colman H, De Groot JF, et al. Orally administered colony stimulating factor 1 receptor inhibitor PLX3397 in recurrent glioblastoma: an Ivy Foundation Early Phase Clinical Trials Consortium phase II study. *Neuro-Oncology* 2016; 18(4):557–564.